



**HAL**  
open science

## Atomistic study of ordinary $\frac{1}{2}\langle 110 \rangle$ screw dislocations in single-phase and lamellar $\gamma$ -TiAl

Ivaylo Hristov Katzarov, Marc Cawkwell, Anthony T Paxton, Michael W  
Finnis

### ► To cite this version:

Ivaylo Hristov Katzarov, Marc Cawkwell, Anthony T Paxton, Michael W Finnis. Atomistic study of ordinary  $\frac{1}{2}\langle 110 \rangle$  screw dislocations in single-phase and lamellar  $\gamma$ -TiAl. *Philosophical Magazine*, 2007, 87 (12), pp.1795-1809. 10.1080/14786430601080252. hal-00513806

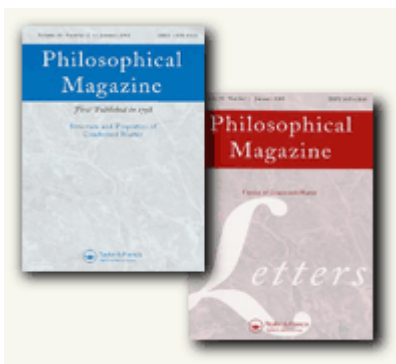
**HAL Id: hal-00513806**

**<https://hal.science/hal-00513806>**

Submitted on 1 Sep 2010

**HAL** is a multi-disciplinary open access archive for the deposit and dissemination of scientific research documents, whether they are published or not. The documents may come from teaching and research institutions in France or abroad, or from public or private research centers.

L'archive ouverte pluridisciplinaire **HAL**, est destinée au dépôt et à la diffusion de documents scientifiques de niveau recherche, publiés ou non, émanant des établissements d'enseignement et de recherche français ou étrangers, des laboratoires publics ou privés.



**Atomistic study of ordinary  $\frac{1}{2}$   $\langle 110 \rangle$  screw dislocations in single-phase and lamellar  $\gamma$ -TiAl**

Journal:	<i>Philosophical Magazine &amp; Philosophical Magazine Letters</i>
Manuscript ID:	TPHM-06-Jun-0231.R2
Journal Selection:	Philosophical Magazine
Date Submitted by the Author:	17-Oct-2006
Complete List of Authors:	Katzarov, Ivaylo; Queen's University, Atomistic Simulation Centre, School of Mathematics and Physics Cawkwell, Marc; Los Alamos National Laboratory Paxton, Anthony; Queen's University, Atomistic Simulation Centre, School of Mathematics and Physics Finnis, Michael; Imperial College, Faculties of Engineering and Natural Sciences
Keywords:	atomistic simulation, dislocations, plasticity of metals, tight-binding, titanium aluminides
Keywords (user supplied):	
<p>Note: The following files were submitted by the author for peer review, but cannot be converted to PDF. You must view these files (e.g. movies) online.</p>	
TiAl-rev-II.tex	



# Atomistic study of ordinary $\frac{1}{2} \langle 110 \rangle$ screw dislocations in single-phase and lamellar $\gamma$ -TiAl

I. H. Katzarov\*, M. J. Cawkwell†, A. T. Paxton\*, M. W. Finnis‡

\* *Atomistic Simulation Centre, School of Mathematics and Physics, Queens University Belfast, Belfast BT7 1NN, Northern Ireland, U.K.*

† *Los Alamos National Laboratory, Los Alamos, NM 87545, USA*

‡ *Department of Materials, Imperial College of Science, Technology and Medicine, Exhibition Road, London SW7 2AZ, U.K.*

## Abstract

Computer simulation of the core structure and glide of ordinary  $\frac{1}{2} \langle 110 \rangle$  screw dislocations in single-phase  $L1_0$  TiAl and in two lamellae forming twin  $\gamma/\gamma$ -interface has been performed using recently constructed Bond-Order Potentials (BOPs). BOPs represent a semi-empirical, numerically efficient scheme that works within the orthogonal tight-binding approximation and is able to capture the directionality of bonding. We have studied dislocation glide in perfect  $L1_0$  TiAl and along a twin interface, transmission of an ordinary screw dislocation between lamellae, and the core structure, mobility and detachment of an interfacial  $\frac{1}{2} \langle 110 \rangle$  screw dislocation from a twin boundary under applied shear stresses in directions parallel and perpendicular to a (111) plane. Our results show that the glide of ordinary  $\frac{1}{2} \langle 110 \rangle$  straight screw dislocations under applied stresses in  $L1_0$  TiAl is characterized by zigzag movement on two conjugated  $\{111\}$  planes. The non-planar core of the  $\frac{1}{2} \langle 110 \rangle$  screw dislocation is distorted asymmetrically when the elastic center of the dislocation is close to a twin  $\gamma/\gamma$ -interface and the dislocation moves on one of the (111) planes, depending on the magnitude of the corresponding Schmid factor. Ordinary dislocations become ordinary interfacial dislocations when they reach the interface. With increasing applied stress they can glide into the adjacent lamella, leaving no remnant interfacial dislocation.

## 1 Introduction

It is due to their low density, exceptionally high strength, hardness, creep resistance and corrosion resistance at high temperatures, that  $\gamma$ -TiAl-based alloys are considered for applications in aerospace and automotive industries. In spite of the promising high-temperature properties, the low ductility and

1  
2  
3  
4  
5  
6  
7  
8 fracture toughness at room temperature have limited their commercial ap-  
9 plication so far. Gamma phase in its single-phase region is very brittle  
10 and therefore has not attracted much industrial interest. An improvement  
11 of ductility and fracture toughness at low temperatures can be achieved  
12 by special heat treatments leading to the formation of a refined two-phase  
13 lamellar structure, consisting of layers of  $\gamma$ -TiAl (tetragonal L1<sub>0</sub>) and  $\alpha_2$ -  
14 Ti<sub>3</sub>Al (hexagonal DO<sub>19</sub>) phases. The lamellar character, surprisingly, leads  
15 to higher room-temperature ductility which is practically zero for TiAl in  
16 the pure  $\gamma$ -phase structure [1, 2, 3]. The improvement of mechanical proper-  
17 ties is evidently due to the presence of lamellar boundaries in the material.  
18 The reasons behind this phenomenon are not fully understood.

19  
20  
21 The ductility of a crystalline material is principally controlled by the in-  
22 teraction of dislocations with the applied stress and with other defects such  
23 as other dislocations, grain boundaries and precipitates. The main deforma-  
24 tion modes in  $\gamma$ -TiAl are slip and twinning, both of which operate on the  
25 close-packed {111} planes [4]. Slip occurs via two types of dislocations: or-  
26 dinary dislocations with Burgers vector  $\frac{1}{2}\langle 110 \rangle$  and  $\langle 101 \rangle$  superdislocations.  
27 The observed twinning is in the  $\eta_1 = \langle 112 \rangle$  direction with composition plane  
28  $K_1 = (111)$ . In single crystals, superdislocations dominate at low tempera-  
29 tures and the glide of ordinary dislocations and twinning become dominant  
30 only at high temperatures [4, 5]. By contrast, in lamellar TiAl twinning is  
31 the prevailing mechanism at room temperature but high density and glide  
32 of  $\frac{1}{2}\langle 110 \rangle$  ordinary dislocations in the  $\gamma$ -lamellae is also observed. The glide  
33 of  $\langle 101 \rangle$  superdislocations becomes significant only at high temperatures [6].

34  
35 To understand the role the interfaces play in enhancing the ductility,  
36 and the difference between deformation mechanisms in single-phase and two-  
37 phase TiAl alloys, we have to gain deeper insight into the mechanisms of  
38 deformation and the transmission of dislocations across the lamellar bound-  
39 aries at the atomic scale. The ductility is controlled predominantly by the  
40 properties of  $\gamma/\gamma$ -interfaces as they are much more frequent than those of  
41 the  $\gamma/\alpha_2$  type, and the  $\alpha_2$  phase is not very deformable. In the complex  
42 lamellar structure the interaction of dislocations with interfaces is very diffi-  
43 cult to analyze by purely analytical or experimental means. There are three  
44 types of  $\gamma/\gamma$ -interface between the different orientation variants of  $\gamma$ -TiAl,  
45 formed by rotating about the [111] axis by angles of 60°, 120° and 180° [6].  
46 A similar orientation-based classification exists also for  $\alpha_2$  interfaces. The  
47 180° interface is also referred to as the twin interface. Only in the case of  
48 the twin formed by a rotation of 180° about the normal to the interface do  
49 the  $\langle 110 \rangle$  directions across the interface remain parallel; hence this inter-  
50 face is fully coherent irrespective of the magnitude of lattice tetragonality.  
51 Twins comprise more than 60% of all  $\gamma/\gamma$ -interfaces [7]. The main reason  
52 is presumably the low energy of twin boundaries [8]. On the other twist  
53 boundaries, with rotations 120° and 60°, a network of interfacial disloca-  
54 tions forms at the lamellar boundaries to compensate the misfit caused by  
55  
56  
57  
58  
59  
60

1  
2  
3  
4  
5  
6  
7  
8 the tetragonality of the  $L1_0$  structure. Such a network also compensates the  
9 misfit between  $\gamma$  and  $\alpha_2$  or forms as a result of the decomposition of im-  
10 pinging crystal dislocations [9]. It is possible that interfacial dislocations are  
11 mobile along the interface or can propagate inside the lamellae, and could  
12 thus increase the number of modes of plastic deformation.

13  
14 The only plausible way of studying such phenomena is by means of com-  
15 puter simulation. A number of computer simulations of the structure and  
16 properties of dislocations in single-phase  $L1_0$ -TiAl have been made by pre-  
17 vious authors [10, 11, 12, 13]. In these studies, central-force potentials were  
18 used to describe the atomic interactions in the material. These do not cap-  
19 ture effects arising from the covalent and directional bonding characteristic  
20 of TiAl. The core structure and friction barrier of the ordinary  $\frac{1}{2} \langle 110 \rangle$  dislo-  
21 cation was also studied using an *ab initio* density-functional theory (DFT)  
22 based method [14]. This approach provides a good description of the inter-  
23 atomic forces, but is limited in the number of atoms that can be simulated.

24  
25 The most important precursor of atomistic simulations of the core struc-  
26 ture and glide of dislocations and dislocation-interface interaction that in-  
27 volve systems composed of a large number of atoms, is a reliable description  
28 of inter-atomic interactions. First-principles methods based on DFT provide  
29 such a description most reliably but are limited by feasible block sizes that  
30 contain not more than a couple of hundred atoms and usually require use of  
31 periodic boundary conditions that are not well suited for dislocation studies.  
32 Recently, a Bond Order Potential (BOP) for  $L1_0$  TiAl was constructed and  
33 tested by a variety of calculations involving large deviations from the ideal  
34  $L1_0$  lattice [15, 16]. BOPs were first formulated by Pettifor and cowork-  
35 ers [17, 18, 19] and represent a numerically efficient scheme that expresses  
36 the orthogonal tight-binding approximation in terms of short-ranged non-  
37 central interatomic potentials [20]. The multi-atom character of the forces  
38 is thereby captured in a physical way that goes beyond the embedded-atom  
39 model for example, and BOPs can describe features such as the negative  
40 Cauchy pressures ( $C_{13} - C_{44} < 0$ ,  $C_{12} - C_{66} < 0$ ) that simpler models  
41 cannot. In the framework of the BOP for TiAl the energy of a system of  
42 atoms is divided into three parts: bond energy  $E^{\text{bond}}$  arising from the for-  
43 mation of the valence band and including terms dependent on bond angles;  
44 repulsive energy  $E^{\text{pair}}$  described by pair interactions, including the Coulomb  
45 repulsion of the nuclei; and an environmentally dependent part of the en-  
46 ergy  $E^{\text{env}}$ , including the overlap repulsion that arises from the valence s, p  
47 electrons, which may be squeezed according to the Pauli principle by over-  
48 lapping orbitals from neighbouring atoms. The tight-binding parameters  
49 entering  $E^{\text{bond}}$  are fitted to *ab initio* DFT data generated with the Tight-  
50 Binding Linear Combination of Muffin Tin Orbitals method (TB-LMTO).  
51  $E^{\text{env}}$  and  $E^{\text{pair}}$  are constructed by fitting the Cauchy pressures and several  
52 equilibrium properties, namely lattice parameters, other elastic moduli and  
53 the cohesive energy [15]. A further advantage of BOPs is that they allow the  
54  
55  
56  
57  
58  
59  
60

1  
2  
3  
4  
5  
6  
7  
8  
9  
10  
11  
12  
13  
14  
15  
16  
17  
18  
19  
20  
21  
22  
23  
24  
25  
26  
27  
28  
29  
30  
31  
32  
33  
34  
35  
36  
37  
38  
39  
40  
41  
42  
43  
44  
45  
46  
47  
48  
49  
50  
51  
52  
53  
54  
55  
56  
57  
58  
59  
60

evaluation of the energy in a computation time that scales linearly with the number of atoms, so that it is feasible to simulate the thousands of atoms needed to study the interaction between dislocations and interfaces. Variants of the BOP method were implemented in the Oxford order-N package (OXON) [21]. Computer simulation of the core structure of ordinary  $\frac{1}{2}\langle 110\rangle$  screw dislocations and  $\langle 101\rangle$  superdislocations has been performed using the recently constructed BOP [16, 22]. The non-planar core of the ordinary  $\frac{1}{2}\langle 110\rangle$  screw dislocation, simulated by using BOP, is in excellent agreement with *ab initio* calculations.

In this paper we present results of atomistic simulations of the core structure and mobility of the ordinary screw  $\frac{1}{2}\langle 110\rangle$  dislocation in single-phase  $L1_0$  TiAl and in two  $\gamma$  lamellae forming a twin  $\gamma/\gamma$ -interface. In our simulations we have used the BOP for TiAl developed in [15]. We study the glide of the  $\frac{1}{2}[1\bar{1}0]$  screw dislocation in  $L1_0$  TiAl and along a twin interface, in a direction parallel to the interface. We then follow the process of transmission of an ordinary screw dislocation between  $\gamma$  lamellae. Finally we study the core structure, mobility and detachment of an interfacial  $\frac{1}{2}[1\bar{1}0]$  screw dislocation from a twin boundary, induced by applied shear stresses in directions parallel and perpendicular to a (111) plane. The aim of such simulations is to gain deeper insight into the  $\frac{1}{2}\langle 110\rangle$  dislocation glide in single-phase  $L1_0$  TiAl and along a twin  $\gamma/\gamma$  lamellar boundary, the mechanisms of transmission of ordinary dislocation across the lamellar boundaries and to elucidate the reasons for the higher density and different behavior of  $\frac{1}{2}\langle 110\rangle$  dislocations in the  $\gamma$ -lamellae compared to non-lamellar  $L1_0$  TiAl. Based on the results of these calculations we suggest reasons for the peculiar dislocation behaviour exhibited by the lamellar  $\gamma$ -phase material.

## 2 Modelling the $\frac{1}{2}\langle 110\rangle$ screw dislocation in $L1_0$ TiAl

In our dislocation calculations the  $L1_0$  TiAl crystal was constructed of two  $(1\bar{1}0)$  planes forming one period in the  $[1\bar{1}0]$  direction, along which periodic boundary conditions were applied. We set the x, y, and z axis of the simulation cell parallel to the  $[\bar{1}\bar{1}2]$ ,  $[111]$ , and  $[1\bar{1}0]$  directions, respectively. The simulation block is divided into two sub-blocks. The positions of atoms in the inner sub-block, which includes the dislocation line, are adjusted so as to attain minimum of the energy (the so-called ‘active atoms’). The atoms in the outer sub-block are kept fixed in the positions of the corresponding perfect lattice (‘inert atoms’).

The  $\frac{1}{2}[1\bar{1}0]$  left handed screw dislocation was introduced by displacing the atoms in both regions from their perfect lattice positions according to the corresponding anisotropic elastic displacement field [23]. A molecular statics method of minimizing the energy of the system was employed. During

1  
2  
3  
4  
5  
6  
7  
8 the relaxation the inert atoms retain their initial displacement while the  
9 active atoms are shifted until a minimum energy configuration is found.  
10 The relaxation was terminated when the force on every atom was smaller  
11 than  $5 \cdot 10^{-2} \text{ eV/\AA}$ .  
12

13 In order to estimate the lattice friction stress we started with a simula-  
14 tion block containing the fully relaxed core structure of a  $\frac{1}{2} [1\bar{1}0]$  ordinary  
15 screw dislocation. To this we have applied an incrementally increasing pure  
16 shear stress in the  $[1\bar{1}0]$  direction on the  $(111)$  plane. In practice this stress  
17 is imposed by applying the appropriate homogeneous shear strain, which is  
18 evaluated with anisotropic elasticity theory. This strain was superimposed  
19 on the dislocation displacement field for all the atoms. Relaxation was car-  
20 ried out at every incremental step in the applied stress, until the dislocation  
21 started to move.  
22

23 The motion of the dislocation is illustrated (Figure 1) by a series of  
24 differential displacement plots [24]. The light and dark circles represent the  
25 positions of Al and Ti atoms, respectively. At zero applied stress a non-  
26 planar core structure of the  $\frac{1}{2} \langle 110 \rangle$  screw dislocation was found, which was  
27 distributed symmetrically on two  $\{111\}$  planes (Fig. 1a). The same core  
28 structure has been reported previously in [14] and [16]. As the shear stress  
29 is applied, the dislocation begins to distort with the displacements extending  
30 asymmetrically along the  $\{111\}$  planes. The stress at which the dislocation  
31 starts to move is the critical resolved shear stress (CRSS) on the slip plane  
32 (the Peierls stress). The magnitude of the CRSS on the  $(111)$  plane we  
33 predict for TiAl is  $0.015C_{44}$  ( $C_{44} = 0.680 \text{ Mbar}$ ). This value is in agreement  
34 with the lattice frictional stress predicted by a DFT method (greater than  
35  $0.01C_{44}$ ) [14].  
36  
37

38 As the dislocation goes over the Peierls barrier (Fig. 1b), its core struc-  
39 ture continues to be non-planar but rather distorted in comparison to the  
40 unstressed core. With the increase of the applied stress above the frictional  
41 barrier the displacements extend along the cross-slip plane. The concen-  
42 tration of strain on the  $(111)$  plane leads to cross-slip of the dislocation  
43 along the conjugated  $(11\bar{1})$  (Fig. 1c). After moving one lattice spacing on  
44  $(11\bar{1})$  the dislocation cross-slips again and starts gliding on the  $(111)$  plane  
45 (Fig. 1d). Similar motion of the ordinary screw dislocation, starting with  
46 glide on  $(11\bar{1})$ , was found when the glide stress was applied on the  $(11\bar{1})$   
47 plane.  
48  
49

50 **The differential displacement plots illustrating a dislocation**  
51 **moving by one lattice spacing along the primary  $(111)$  plane are**  
52 **very similar to the previous DFT calculations of the same system,**  
53 **using a flexible boundary condition method [14]. An interesting**  
54 **characteristic of the glide of the  $\frac{1}{2} \langle 110 \rangle$  screw dislocation in an**  
55 **ideal  $L1_0$  TiAl crystal, predicted by BOP for TiAl, is the cross-**  
56 **slip of the ordinary dislocation on the conjugated  $(11\bar{1})$  plane after**  
57 **moving by one lattice spacing along the primary  $(111)$  plane. The**  
58  
59  
60

1  
2  
3  
4  
5  
6  
7  
8 cross-slip of the ordinary dislocation after the first step along the  
9 primary plane can not be confirmed by the previous *ab initio*  
10 calculations, because the DFT simulations do not report results  
11 for the dislocation behaviour in response to increase of the applied  
12 stress above the CRSS.  
13

14 The discrepancy between the critical resolved shear stresses  
15 predicted by BOP and DFT methods as well as the zigzag mo-  
16 tion of the dislocation may be due to the size of the cell used in  
17 the simulations. Although artifacts arising from the use of fixed  
18 boundary conditions cannot be excluded entirely, we used five dif-  
19 ferent simulation cells to model the motion of the dislocation in  
20 order to determine the sensitivity of the critical resolved shear  
21 stress and the dislocation motion to the size of the simulation cell.  
22 The calculations described here, are performed with supercells  
23 of 210, 288, 1680, 2208 and 2520 active atoms. The results ob-  
24 tained from all five simulation cell sizes are qualitatively similar;  
25 the Peierls stresses agree to within a margin of error of  $0.001C_{44}$ .  
26 In particular, there is no observed decrease in the Peierls stress  
27 associated with an increase in cell size.  
28  
29  
30

### 31 32 **3 The $\frac{1}{2} \langle 110 \rangle$ ordinary screw dislocation in lamellar** 33 **L1<sub>0</sub> TiAl** 34

#### 35 36 **3.1 Core structures and friction stress along a $\gamma$ -phase twin** 37 **boundary** 38

39 A rectangular parallelepiped simulation cell was used in all simulations  
40 of dislocation-twin boundary interactions. To simulate the interaction of  
41  $\frac{1}{2} [1\bar{1}0]$  screw dislocations with  $\gamma$ -phase twin boundaries, the size of the sim-  
42 ulation cell was 26 atomic layers along the  $[111]$  direction, 55 nm along the  
43  $[112]$  direction and one periodic unit along the  $[1\bar{1}0]$  direction. To introduce  
44 the twin boundary, the upper half of the block was rotated with respect  
45 to the lower by  $180^\circ$  about the  $[111]$  direction. As before, the simulation  
46 cell was divided into an inner region of active atoms and an outer, fixed  
47 region, with periodic boundary conditions parallel to the dislocation line.  
48 The simulation block consists of 336 active and 456 inert atoms. Initially,  
49 the cell was relaxed to allow for atomic rearrangement at or near the inter-  
50 face. A dislocation was introduced into the simulation cell after the initial  
51 relaxation by displacing all atoms according to the anisotropic elastic dis-  
52 placement field of a dislocation on a planar interface [26]. We illustrate in  
53 Fig. 2a and Fig. 2b the dislocation core structures found for two  $\frac{1}{2} [1\bar{1}0]$   
54 screw dislocations with their initial elastic centers introduced at different  
55 distances from the twin boundary. The cores are non-planar, distorted near  
56  
57  
58  
59  
60

1  
2  
3  
4  
5  
6  
7  
8 the interface, and the extensions into the  $(11\bar{1})$  plane are asymmetrical. The  
9 concentration of strain on the twin boundary increases as the elastic centers  
10 of the dislocations approach the boundary. With no applied strain, the core  
11 is neither attracted nor repelled from the boundary. This result is not sur-  
12 prising, because twin boundaries do not introduce coherency stresses or any  
13 elastic constant mismatch, which otherwise could induce forces on a lattice  
14 dislocation in the lamellae.

15  
16 A series of calculations at various applied strains was used to determine  
17 the frictional barrier and motion of the dislocation, starting with its elastic  
18 center in the upper lamella one atomic layer away from the boundary (Fig.  
19 2b). The sense of the shear strain is such that the force on the dislocation  
20 pushes it in  $[\bar{1}\bar{1}2]$  (with respect to the lower crystal) direction, parallel to the  
21 interface. The motion of the dislocation is illustrated (Figure 3) in a series  
22 of differential displacement plots. In contrast to its motion in the perfect  
23 crystal, the dislocation core structure along a twin interface is only very  
24 slightly distorted as the dislocation goes over the Peierls barrier (Fig.3b)  
25 and it continues gliding parallel to the boundary as the applied stress is  
26 raised. When the dislocation moves it has to stay in the  $(111)$  plane as  
27 there is no continuation of the  $(11\bar{1})$  plane across the interface. If the glide  
28 force applied to the dislocation is reversed it still moves on the  $(111)$  plane,  
29 but due to the asymmetric core structure the frictional stress in the  $[11\bar{2}]$   
30 direction is lower ( $0.024C_{44}$ ) than in the  $[\bar{1}\bar{1}2]$  direction.  
31  
32  
33  
34

### 35 3.2 The barrier strength of a $\gamma$ -phase twin boundary

36 To simulate the mechanism of transmission of a  $\frac{1}{2} \langle 110 \rangle$  screw dislocation  
37 through a twin boundary and to determine the blocking strength of the  
38 boundary to this dislocation, we again applied an increasing shear strain to  
39 the initially relaxed configuration described in Section 3.1. As before, the  
40 dislocation was initially located one atomic layer from the boundary (Fig.  
41 2b). This time the sense of the applied shear strain was such that the force  
42 on the dislocation pushes it towards the boundary. The stress at which a  
43 dislocation overcomes the obstacle presented by the interface is its "barrier  
44 strength". Since the  $(11\bar{1})$  slip planes in the two lamellae are not continuous  
45 across the boundary, the dislocation has to cross-slip for transmission of  
46 slip across the boundary. As a result, the blocking strength of the twin  
47 boundary is expected to be substantially larger than the friction stress in an  
48 ideal crystal, and competing processes such as indirect transmission of slip  
49 across the boundary become more probable.  
50  
51  
52

53 At an applied stress of  $0.015C_{44}$ , the screw dislocation moves close to the  
54 lamellar boundary and is blocked (Fig. 4a). The core structure is distorted  
55 significantly and spread asymmetrically within the boundary and in  $(11\bar{1})$   
56 planes on either side. The concentration of strain on the  $(11\bar{1})$  plane in the  
57 second crystal is displaced along the boundary from the intersection between  
58  
59  
60

1  
2  
3  
4  
5  
6  
7  
8 the boundary and the  $(11\bar{1})$  plane on which the strain in the first lamella is  
9 concentrated. The concentration of strain on the  $(11\bar{1})$  plane in the second  
10 lamella increases with increasing applied stress (Fig. 4b). At an applied  
11 stress of  $0.0417C_{44}$  (Fig. 4c), the dislocation overcomes the obstacle and  
12 moves into the second lamella. Since the transmission of the dislocation  
13 takes place at a stress much higher than the friction barrier in the perfect  
14 crystal, our molecular static approach, whereby the energy of the system  
15 is minimized, does not allow us to trace the propagation of the dislocation  
16 immediately after its detachment from the interface. However, an analysis  
17 of the position of the dislocation after it has passed through the boundary  
18 shows that its path in the second lamella follows the same type of zigzag  
19 motion on  $(111)$  and  $(11\bar{1})$  planes that was observed in the ideal crystal. The  
20  $(11\bar{1})$  plane in the second lamella with the highest strain concentration is the  
21 initial glide plane for the dislocation after crossing the boundary. This plane  
22 is displaced along the interface from the intersection with the interface of the  
23  $(11\bar{1})$  active slip system in the first crystal. Due to the high magnitude of  
24 the applied stress the distortion of the core structure observed in the second  
25 lamella is even bigger than that observed in the perfect crystal.  
26  
27  
28  
29

## 30 4 $\frac{1}{2} \langle 110 \rangle$ Interfacial dislocations

### 31 4.1 Core structure

32  
33 Interfacial dislocations may arise to compensate misfit between orientation  
34 variants with  $120^\circ$  and  $60^\circ$  rotations, to compensate small grown-in de-  
35 viations from the exact crystallographic misorientation, or as a result of  
36 decomposition of impinging crystal dislocations. The structures of the twin  
37 boundaries on  $(111)$  are preserved by displacements equal to the Burgers  
38 vector of the ordinary dislocation [25]. Therefore, the Burgers vectors of  
39 the ordinary dislocations are also Burgers vectors of interfacial dislocations,  
40 sometimes called DSC dislocations, at the twin boundary. In particular, the  
41 Burgers vector of a  $\frac{1}{2} \langle 110 \rangle$  screw twin  $\gamma/\gamma$ -interfacial dislocation is parallel  
42 to the boundary. It can be anticipated that this type of interfacial disloca-  
43 tion is mobile along the interface, and could thus increase the ease of plastic  
44 deformation, consequently increasing the desired toughness of the material.  
45 Due to the orientation of the  $\frac{1}{2} \langle 110 \rangle$  interfacial dislocations with respect to  
46 the crystal interior they do not need to be attached to the interface but can  
47 propagate inside the lamellae when an appropriate glide stress is applied.  
48  
49

50  
51 To determine the core structures and mobility of a  $\frac{1}{2} \langle 110 \rangle$  screw inter-  
52 facial dislocation, it was introduced into a simulation cell containing a  $180^\circ$   
53 twin boundary in the way described previously. The relaxed structure of the  
54  $\frac{1}{2} [1\bar{1}0]$  screw interfacial dislocation at a twin interface is shown in Fig. 5a us-  
55 ing the method of differential displacements. As before, the non-planar core  
56 structure spread asymmetrically into the boundary and  $(11\bar{1})$  planes in both  
57  
58  
59  
60

1  
2  
3  
4  
5  
6  
7  
8 lamellae. The concentration of strain on the  $(11\bar{1})$  plane in the upper crystal  
9 is displaced along the interface from the intersection with the interface of  
10 the  $(11\bar{1})$  plane on which the strain in the lower crystal is concentrated. No  
11 dissociation of the interfacial  $\frac{1}{2}\langle 110\rangle$  screw dislocation into Shockley partials  
12 separated by the complex stacking fault (CSF) was observed. The reason is  
13 presumably the high energy of the CSF ( $550\text{ mJ/m}^2$ ) at the twin boundary,  
14 which is even higher than the energy of the CSF ( $412\text{ mJ/m}^2$ ) calculated  
15 in bulk  $L1_0$  TiAl [8, 16]. The motion of the dislocation on applying a pure  
16 shear stress in the  $[1\bar{1}0]$  direction on the  $(111)$  plane is illustrated (Fig. 5)  
17 in a series of differential displacement plots. The sense of the applied shear  
18 strain was to produce a glide force in the  $[11\bar{2}]$  direction. The interfacial dis-  
19 location starts to move on the interface in this direction at an applied stress  
20 of  $0.028C_{44}$  (Fig. 5b). As the dislocation moves through one lattice spacing  
21 along  $[11\bar{2}]$  its core structure is not distorted compared to the configuration  
22 it had without stress, and it continues gliding on the boundary as the ap-  
23 plied stress is increased above the friction barrier. Unlike the case of the  
24  $\frac{1}{2}\langle 1\bar{1}0\rangle$  screw dislocation moving in the  $[11\bar{2}]$  direction we found considerable  
25 distortion of the core structure on reversing the sense of the glide force. On  
26 increasing the applied stress the interfacial dislocation tends to detach from  
27 the boundary. No glide of the ordinary interfacial screw dislocation along  
28 the interface in the  $[\bar{1}\bar{1}2]$  direction was predicted by BOP for TiAl.

## 33 4.2 Transformation to a lattice dislocation

34 To simulate the detachment of the interfacial  $\frac{1}{2}\langle 110\rangle$  screw dislocation from  
35 the twin boundary, its transformation to a lattice dislocation and propaga-  
36 tion inside the crystal interior, we applied a stepwise increasing shear strain  
37 to the initially relaxed interfacial dislocation core structure (Fig. 5a). Simi-  
38 larly to the case of transmission of dislocations through a lamellar boundary,  
39 the applied shear strain is perpendicular to the interface and induces a glide  
40 force in the  $[\bar{1}\bar{1}\bar{1}]$  direction. The core structure starts to distort at an applied  
41 stress of  $0.020C_{44}$  (Fig. 6a). When the applied stress exceeded  $0.025C_{44}$ , the  
42 core structure spreads into the twin boundary and two  $\{111\}$  planes in the  
43 lower lamella and the interfacial dislocation transformed to a lattice  $\frac{1}{2}\langle 110\rangle$   
44 screw dislocation with its elastic center displaced several atomic layers away  
45 from the boundary (Fig. 6c). The core structure is distorted compared to  
46 the core of ordinary dislocations along the interface (Fig. 2) due to the  
47 applied stress.

48 Comparison between Fig. 4a and Fig. 5a shows that when ordinary dis-  
49 locations reach the boundary they become ordinary interfacial dislocations.  
50 Hence, the mechanism of transmission of a  $\frac{1}{2}\langle 110\rangle$  screw dislocation through  
51 a twin boundary after the formation of interfacial dislocation is similar to  
52 the mechanism of detachment of the interfacial  $\frac{1}{2}\langle 110\rangle$  screw dislocation  
53 from the interface. The difference between the two cases is due to the high  
54  
55  
56  
57  
58  
59  
60

1  
2  
3  
4  
5  
6  
7  
8 applied stress in the simulation block necessary for the formation of the  
9 interfacial dislocation in Fig. 4a, as an intermediate step of the transmis-  
10 sion of the dislocation into the adjacent lamella. As a result, the interfacial  
11 dislocation shown in Fig. 5a detaches from the boundary at a lower stress  
12 than the stress necessary for the transmission of ordinary screw dislocation  
13 through the interface (Fig. 4). In the case of lower stress applied in the lat-  
14 tice, the molecular statics method allows us to trace better the propagation  
15 of the detaching dislocation in the second crystal. While the proximity of  
16 the boundary distorts asymmetrically the core structure of the dislocation,  
17 with increasing stress the displacements extend along the  $(11\bar{1})$  slip plane  
18 (Fig. 6b). Several atomic layers away from the interface, the ordinary dis-  
19 location recovers its typical core structure, spreading into two  $\{111\}$  planes  
20 (Fig. 6c) and its glide again becomes a zigzag motion on  $(111)$  and  $(11\bar{1})$   
21 planes. It may be supposed that the propagation of the dislocation in the  
22 second lamella when it is transmitted through the boundary is completely  
23 analogous.  
24  
25  
26  
27

## 28 5 Discussion

29  
30 Our atomistic simulation results for  $L1_0$  TiAl show that the glide of ordi-  
31 nary  $\frac{1}{2}\langle 110\rangle$  straight dislocations in the screw orientation under an applied  
32 stress is characterized by zigzag movement on two conjugated  $\{111\}$  planes.  
33 When the dislocation moves by one lattice spacing along the primary  $(111)$   
34 plane its core structure at the new location is rather distorted, compared to  
35 its initial configuration, due to the high resolved shear stress. The distorted  
36 core structure leads to cross slip of the ordinary dislocation on the  $(11\bar{1})$   
37 plane with increasing stress. The combination and succession of the cross  
38 slip planes depends on the orientation of the applied shear stress and on  
39 the magnitude of the corresponding Schmid factors. The same motion in  
40 between  $(111)$  and  $(11\bar{1})$  planes was found even if the Schmid factor for one  
41 of the planes is zero. The non-planar core of the  $\frac{1}{2}\langle 110\rangle$  screw dislocation,  
42 spread into two planes of the  $\{111\}$  type, is distorted asymmetrically when  
43 the elastic center of the dislocation is close (within 2-3 atomic layers) to a  
44 twin boundary. While the proximity of the interface distorts the core struc-  
45 ture of the dislocation, it moves on just one or other of the  $(111)$  planes,  
46 depending on the magnitude of the corresponding Schmid factor. We there-  
47 fore see two glide mechanisms, depending on how close the dislocation lies to  
48 a twin boundary. Due to the asymmetric core structure close to the bound-  
49 ary the frictional barriers for  $(111)$  glide in  $[\bar{1}\bar{1}2]$  and  $[11\bar{2}]$  directions are  
50 different. The dislocation starts to move under an applied stress of  $0.027C_{44}$   
51 in  $[\bar{1}\bar{1}2]$  and  $0.024C_{44}$  in the opposite direction.  
52  
53  
54  
55

56 **The zigzag motion of the dislocation leading on average to**  
57 **glide on the  $(001)$  plane as predicted by our BOP simulations has**  
58  
59  
60

1  
2  
3  
4  
5  
6  
7  
8 not been observed in practice in TiAl. The reasons for this dis-  
9 crepancy have yet to be clarified. It may be due to several factors.  
10 The second step along  $(11\bar{1})$  plane is not confirmed by DFT sim-  
11 ulations and may be effect of the potential or the fixed boundary  
12 conditions used in the simulations. The results of the atomistic  
13 simulations describing the glide of a  $\frac{1}{2}\langle 110\rangle$  screw dislocation and  
14 its Peierls stress are for straight dislocations in stoichiometric ma-  
15 terial at  $0^\circ$  K. Real dislocations are always in the shape of loops  
16 and their mixed part must stay in the glide plane. The results  
17 of our atomistic simulations indicate that the second step on the  
18 cross-slip plane is due to the distortion of the dislocation core  
19 structure after moving one lattice spacing on the primary plane  
20 as a result of the high critical resolved shear stress. Both BOP  
21 and DFT simulations of straight dislocations predict values for the  
22 critical resolved shear stress more than twice the extrapolated ex-  
23 perimental value at low temperature. The reasons behind this are  
24 not well understood. This may be because the lattice frictional  
25 stress is large enough to favour movement by kink-pair formation.  
26 Solid-solution softening in TiAl alloys can also be caused by de-  
27 viations from stoichiometry [28]. At lower stress the dislocation  
28 core structure of the screw segments will be less distorted and the  
29 first step along  $(111)$  can repeat itself with increasing stress [29].

30  
31  
32  
33  
34 However, there is much experimental evidence that the double  
35 cross slip of the screw segments, predicted by BOP, is an essential  
36 characteristic of the glide of ordinary dislocations. TEM analyses  
37 [30, 31, 32] of ordinary dislocations under stress have shown that  
38 they are elongated along their screw orientation and anchored at  
39 many points. The screw segments separated by pinning points  
40 are observed to lie in different planes, implying that they have  
41 cross slipped onto parallel  $(111)$  planes [32]. The experimental  
42 observations show a dislocation structure more consistent with  
43 dislocation glide involving propagation of macro-kinks, formed as  
44 a result of frequent double cross slip. If no obstacle opposes the  
45 lateral propagation of the edge segments lying in the cross slip  
46 plane, the whole dislocation moves onto a primary glide plane  
47 parallel to the initial one and no trace of cross-slip can be seen.  
48 If the same dislocation makes the same double cross slip but in a  
49 crystal containing extrinsic obstacles, the micrographs show for-  
50 mation of pinning points and several segments of dislocations lying  
51 in different planes. The models explaining the experimental re-  
52 sults require that the ordinary screw dislocation will easily cross  
53 slip, and that the lattice frictional stress is large enough to favour  
54 movement by kink-pair formation. The present 2D simulations can  
55 not provide the necessary information about the core structures of screw  
56  
57  
58  
59  
60

1  
2  
3  
4  
5  
6  
7  
8  
9  
10  
11  
12  
13  
14  
segment containing kinks or jogs, their response to applied stress and influence on the mobility of ordinary screw dislocations. Three dimensional simulations of the activation and propagation of dislocations in nonlamellar and lamellar crystal would be required to fully understand the influence of the two different predicted glide mechanisms on the macroscopic yield in single-phase and lamellar  $\gamma$ -TiAl.

15  
16  
17  
18  
19  
20  
21  
22  
23  
24  
25  
26  
27  
28  
29  
30  
31  
32  
33  
The lamellar interfaces have two-fold functions in the deformation of lamellar crystals of TiAl. The lamellar boundaries are large reservoirs of dislocations, which may assist plastic deformation. However, these interfaces oppose the activation of deformation systems. The results addressed in the previous sections indicate that ordinary dislocation slip can be activated inside the  $\gamma$  lamellae. However, the confinement of the lamellar interfaces leads to the highly anisotropic deformation behaviour. Inui et al. [6] reports two deformation modes for polysynthetically twinned crystals of TiAl: an easy mode, characterized by glide parallel to the lamellar boundaries, and a hard mode, characterized by glide perpendicular to the interfaces. In agreement with this observation, the present atomistic simulation results predict that the mobility of lattice  $\frac{1}{2}\langle 110 \rangle$  screw dislocations close to a twin interface in a direction parallel to the interface is higher than in the perpendicular direction. The mobility of both the lattice and interfacial ordinary dislocations along the interface could thus increase plastic deformation in this direction.

34  
35  
36  
37  
38  
39  
40  
41  
42  
43  
44  
45  
46  
47  
48  
49  
50  
51  
52  
53  
The coherency stresses at the twin lamellar interface can exert a Peach-Köhler force acting on the glide dislocations, which attracts or repels dislocations from the interface. Similar forces do not act on ordinary dislocations in screw orientation and in accordance with this elastic interaction of the dislocations with the interfaces were not predicted by the atomistic simulations. It can be seen from the results presented in the previous sections, that the coherency stresses do not induce non-glide stresses, which modify the core structure of the ordinary screw dislocations (Fig. 2a). In addition to elastic interactions between the lamellar boundaries and the gliding dislocations, the stacking-fault energy changes at the interface ('chemical' or 'gamma surface' mismatch) can result in dislocation core structure changes as the dislocation moves from one lamella to the next. Since the energy of the CSF at the twin boundary is even higher than the energy of the CSF calculated in bulk  $L1_0$  TiAl, the ordinary screw dislocation retains its non-planar core structure as the dislocation approaches the interface and no dissociation into Shockley partials separated by CSF at the interface was predicted by the atomistic simulations.

54  
55  
56  
57  
58  
59  
60  
For this particular crystallographic orientation of the  $\gamma$  lamellae, under an applied stress ordinary dislocations can glide through the twin boundaries. Their Burgers vectors are ordinary on both sides of the interface. In absence of gamma surface and long-range elastic interactions, the blocking strength of the twin interface to the glide of ordinary dislocations is a re-

1  
2  
3  
4  
5  
6  
7  
8  
9  
10  
11  
12  
13  
14  
15  
16  
17  
18  
19  
20  
21  
22  
23  
24  
25  
26  
27  
28  
29  
30  
31  
32  
33  
34  
35  
36  
37  
38  
39  
40  
41  
42  
43  
44  
45  
46  
47  
48  
49  
50  
51  
52  
53  
54  
55  
56  
57  
58  
59  
60

sult of the discontinuity of the slip planes across the interface. As a result, the ordinary screw dislocations have to cross-slip for transmission of slip across the interface. The blocking strength of twin boundaries to the glide of  $\frac{1}{2}\langle 110\rangle$  screw dislocations is found to exceed  $0.040C_{44}$ . When ordinary dislocations reach the boundary they become ordinary interfacial dislocations. These dislocations can glide further in the adjacent lamella under an increasing applied stress, because the directions of their Burgers vectors on either of the twin boundary coincide. In agreement with TEM observations and empirical slip transmission rules [33, 34] the atomistic simulation of ordinary dislocation transfer to the adjacent lamella takes place without any dislocations remaining on the interface. Ordinary screw dislocations recover their typical core structure once they have left the boundary, spreading into two  $\{111\}$  planes, and their glide again becomes a zigzag motion on  $(111)$  and  $(11\bar{1})$  planes.

Following the above calculations we may speculate on a mechanism for the increased number of ordinary dislocations observed within a lamellar structure. The higher density of ordinary dislocations in the lamellar microstructure can be interpreted through the effect of the interfaces, where a very high density of ordinary interfacial dislocations is found [35]. Most probably the reason for the high density of ordinary interfacial dislocations is the decomposition of the superdislocations with a Burgers vector of type  $\langle 101\rangle$  into ordinary dislocations at the lamellar interface. The transformation of a superdislocation into two ordinary dislocations at a lamellar interface is allowed for twin and other orientations, when the Burgers vector of the superdislocation is parallel to the interface [35]. Detachment of ordinary interfacial dislocations, accumulated at the lamellar boundaries, and their propagation into the interior of the lamellae could be one of the possible reasons for the experimentally observed higher density of ordinary dislocations in lamellar than in non-lamellar TiAl at low temperature.

**ACKNOWLEDGEMENTS** This research was supported by the EP-SRC grant no. EP/C015649/1. The authors wish to thank Prof. V. Vitek of University of Pennsylvania for helpful discussions during the course of this work.

## References

- [1] Kim, Y.-W., 1989, Intermetallic alloys based on gamma titanium aluminide. JOM 41, 24.
- [2] Appel, F., Wagner, R., Mater. Sci. Eng. R22, 1998, 187.

- 1  
2  
3  
4  
5  
6  
7  
8 [3] Yamaguchi et al., 1995, in "High-Temperature Intermetallic Alloys VI,  
9 Part 1", edited by J. A. Horton et al., Mat. Res. Soc. Symp. Proc., vol.  
10 364, (Pittsburgh, PA: Materials Research Society), p. 3  
11  
12 [4] M. Yamaguchi, H. Inui, S. Yokoshima, K. Kishida and D. R. Johnson,  
13 Mat. Sci. Eng. A 213, 1996, 25.  
14  
15 [5] Inui, H., Matsumuro, M., Wu, D.-H., and Yamaguchi, M., Phil. Mag. A  
16 75, 1997, 395.  
17  
18 [6] Inui H., Oh M. H., Nakamura A., and Yamaguchi M., Phil. Mag. A 66,  
19 1992, 539.  
20  
21 [7] S. Zghal, S. Naka, A. Couret, Acta Mater. A 45, 1997, 3005.  
22  
23 [8] C.L. Fu and M.H. Yoo, Scripta Mater. 37, 1997, 1453.  
24  
25 [9] V. Paidar, S. Zghal, A. Couret, Mater. Sci. Forum 294-296, 1999, 385.  
26  
27 [10] A. Girshick and V. Vitek, High-Temperature Ordered Intermetallic Al-  
28 loys VI, edited by J. Horton, I. Baker, S. Hanada, R. D. Noebe and D.  
29 Schwartz (Pittsburgh, Materials Research Society), Vol. 364, 1995, 145.  
30  
31 [11] R. Mahapatra, A. Girshick, D. P. Pope and V. Vitek, Scripta Metall.  
32 et Mat. 33, 1995, 1921.  
33  
34 [12] Simmons, J. P., Rao, S. I., and Dimiduk, D. M., Philos. Mag. A 75,  
35 1997, 1299.  
36  
37 [13] J. Panova and D. Farkas, Philos. Mag. A 78, 1998, 389.  
38  
39 [14] C. Woodward and S. I. Rao, Phil. Mag. A 84, 2004, 401.  
40  
41 [15] Znam S., D. Nguuyen-Manh, Pettifor D.G. and Vitek V., Phil. Mag.,  
42 83, 2003, 415.  
43  
44 [16] Znam, S., 2001, Ph.D. Thesis, University of Pennsylvania.  
45  
46 [17] Pettifor D.G., Phys. Rev. Lett. 63, 1989, 2480.  
47  
48 [18] Aoki M. and Pettifor D.G., in Physics of Trans. Metals, edited by P.M.  
49 Oppeneer and J. Kubler -World Scientific, Singapore, 1993, 299.  
50  
51 [19] D. G. Pettifor, I. I. Oleinik, D. Nguyen-Manh and V. Vitek, Comp.  
52 Mat. Sci. 23, 2002, 33.  
53  
54 [20] Finnis M., Interatomic Forces in Condensed Matter, Oxford University  
55 Press, 2003.  
56  
57 [21] Horsfield A.P., Bratkovsky A.M., Fearn M., Pettifor D.G., and Aoki  
58 M., Phys. Rev. B 53, 1996, 12694.  
59  
60

- 1  
2  
3  
4  
5  
6  
7  
8 [22] R. Porizek, S. Znam, D. Nguyen-Manh, V. Vitek and D. G. Pettifor,  
9 Mat. Res. Soc. Symp.Proc. vol. 753, 2003, BB4.3.1.  
10  
11 [23] Hirth, J. P. and Lothe, J., Theory of Dislocations, 2nd edn. Wiley-  
12 Interscience, New York, 1982.  
13  
14 [24] Vitek, V., Cryst. Lattice Defects, 5, 1974, 1.  
15  
16 [25] V. Paidar, J. of Alloys and Compounds 378, 2004, 89.  
17  
18 [26] D. M. Barnett and J. Lothe, J. Phys. F: Metal Phys., Vol. 4, 1974,  
19 1618.  
20  
21 [27] Inui, H., Matsumuro, M., Wu, D. H., and Yamaguchi, M., 1997, Phil.  
22 Mag. A, 75, 395.  
23  
24 [28] Sriram, S., Vasudevan, V. K., and Dimiduk, D. M., 1995, Mater Sci.  
25 Engng, A193, 217.  
26  
27 [29] Vitek, V.,(2006, private communication).  
28  
29 [30] Sriram, S., Dimiduk, D. M., Hazzledine, P. M., and Vasudevan, V. K.,  
30 1997, Phil. Mag.,76, 965.  
31  
32 [31] Viguier B, Hemker KJ, Bonneville J, Louchet F, Martin JL. Phil. Mag.  
33 A 1995, 71, 1295.  
34  
35 [32] A. Couret, Intermetallics 9, 2001, 899.  
36  
37 [33] Hu D., Loretto M.H., Intermetallics, 7, 1999, 1299.  
38  
39 [34] S. Zghal, A. Coujou, A. Couret, Phil. Mag. A 81, 2001, 345.  
40  
41 [35] L. Parrini, J. of Alloys and Compounds 270, 1998, 203.  
42  
43  
44  
45  
46  
47  
48  
49  
50  
51  
52  
53  
54  
55  
56  
57  
58  
59  
60

**FIGURE CAPTIONS**

Fig. 1a-d. Differential displacement plots showing the screw components of a  $\frac{1}{2}\langle 110\rangle$  screw dislocation moving under a pure (111) glide stress. The open circle marks the original position of the dislocation.

Fig. 1a. Applied stress  $\sigma_{zy} = 0$

Fig. 1b. Applied stress  $\sigma_{zy} = -0.015C_{44}$

Fig. 1c. Applied stress  $\sigma_{zy} = -0.017C_{44}$

Fig. 1d. Applied stress  $\sigma_{zy} = -0.020C_{44}$

Fig. 2a, b. Differential displacement plots showing the screw components of the predicted equilibrium dislocations cores for  $\frac{1}{2}\langle 110\rangle$  screw dislocations in TiAl along a twin  $\gamma/\gamma$ -interface. The open circle marks the original position of the elastic centers of dislocations.

Fig. 3a-b. Differential displacement plots showing the screw components of a  $\frac{1}{2}\langle 110\rangle$  screw dislocations moving along a twin  $\gamma/\gamma$ -interface under a pure (111) glide stress.

Fig. 3a. Applied stress  $\sigma_{zy} = -0.020C_{44}$

Fig. 3b. Applied stress  $\sigma_{zy} = -0.027C_{44}$

Fig. 4a-c. Differential displacement plots of the relaxed configurations of  $\frac{1}{2}\langle 110\rangle$  screw dislocations in a  $\gamma/\gamma$  bilayer simulation cell at applied stresses in direction toward the interface.

Fig. 4a. Applied stress  $\sigma_{zx} = -0.015C_{44}$

Fig. 4b. Applied stress  $\sigma_{zx} = -0.040C_{44}$

Fig. 4c. Applied stress  $\sigma_{zx} = -0.0417C_{44}$

Fig. 5a-b. Differential displacement plots showing the screw components of a  $\frac{1}{2}\langle 110\rangle$  interfacial screw dislocations moving along a twin  $\gamma/\gamma$ -interface under a pure (111) glide stress.

Fig. 5a. Applied stress  $\sigma_{zy} = 0$

Fig. 5b. Applied stress  $\sigma_{zy} = 0.028C_{44}$

Fig. 6a-c. Differential displacement plots of the relaxed configurations of  $\frac{1}{2}\langle 110\rangle$  screw interfacial dislocations detaching from the lamellar boundary at applied stresses in direction perpendicular to the interface.

Fig. 6a. Applied stress  $\sigma_{zx} = -0.020C_{44}$

Fig. 6b. Applied stress  $\sigma_{zx} = -0.025C_{44}$

Fig. 6c. Applied stress  $\sigma_{zx} = -0.032C_{44}$

1  
2  $(111)$

3  
4  
5  
6  
7  
8  
9  
10  
11  
12  
13  
14  
15  
16  
17  
18  
19  
20  
21  
22  
23  
24  
25

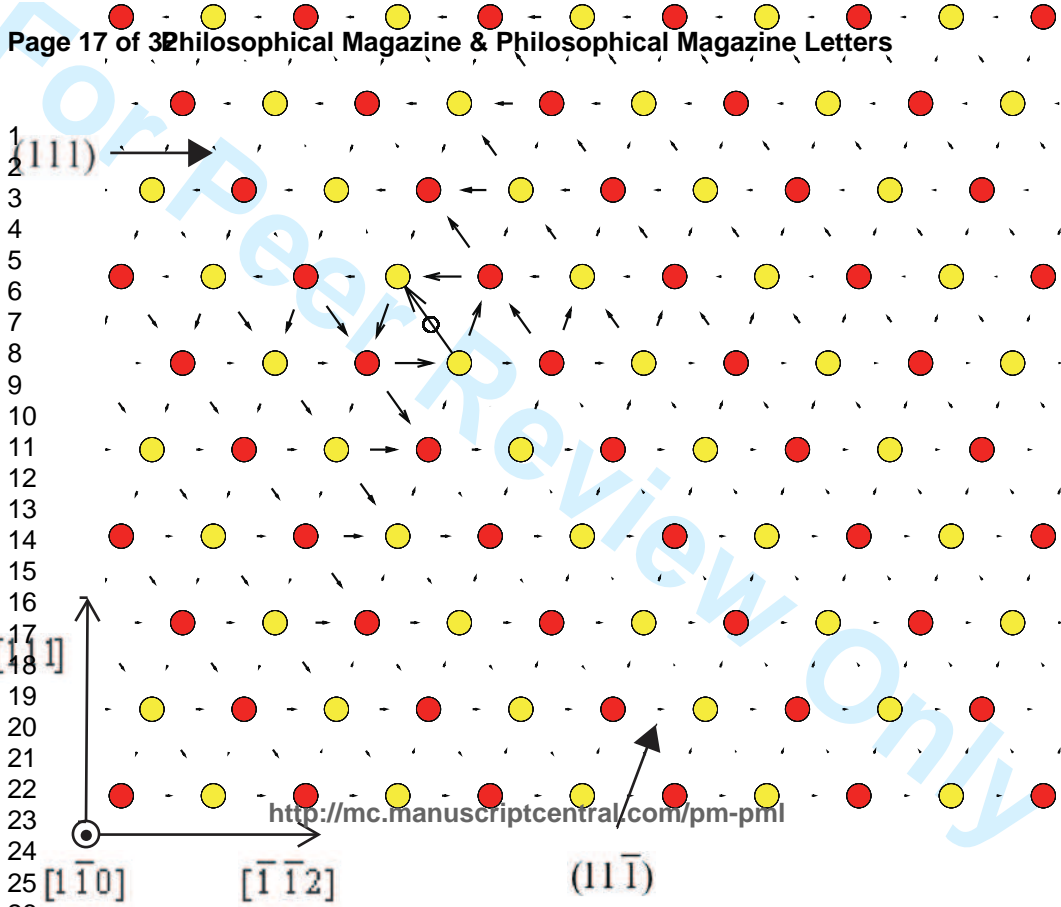
$[1\bar{1}1]$

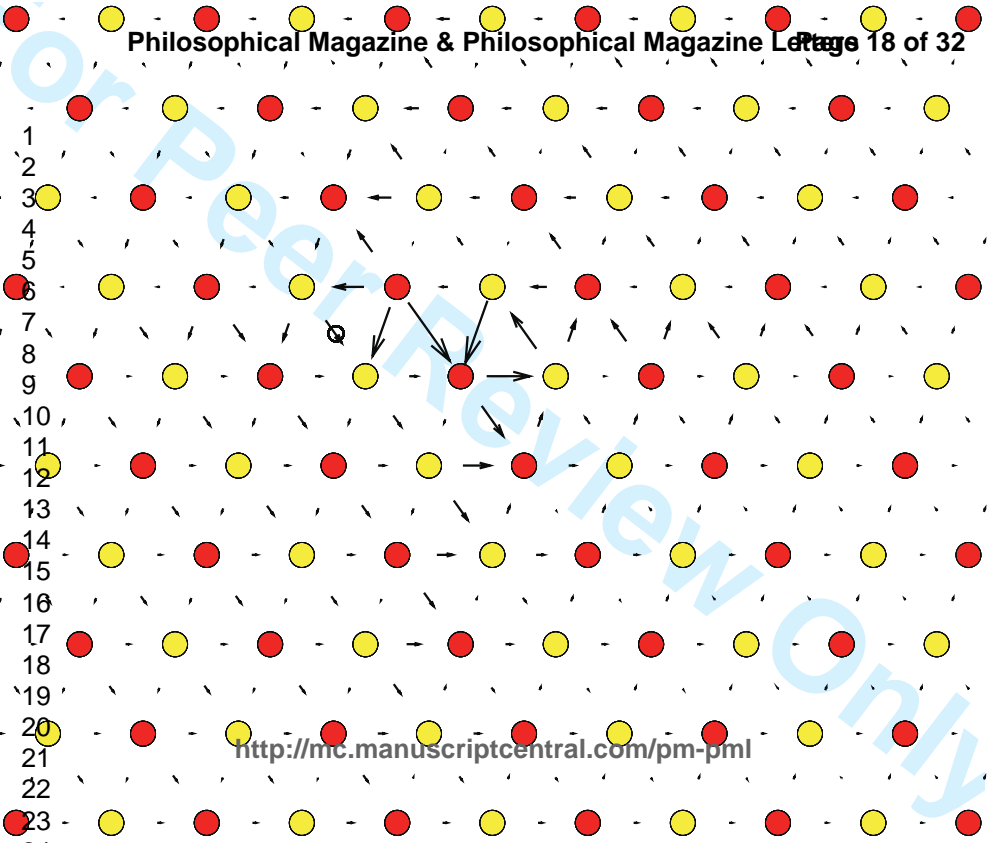
$[1\bar{1}0]$

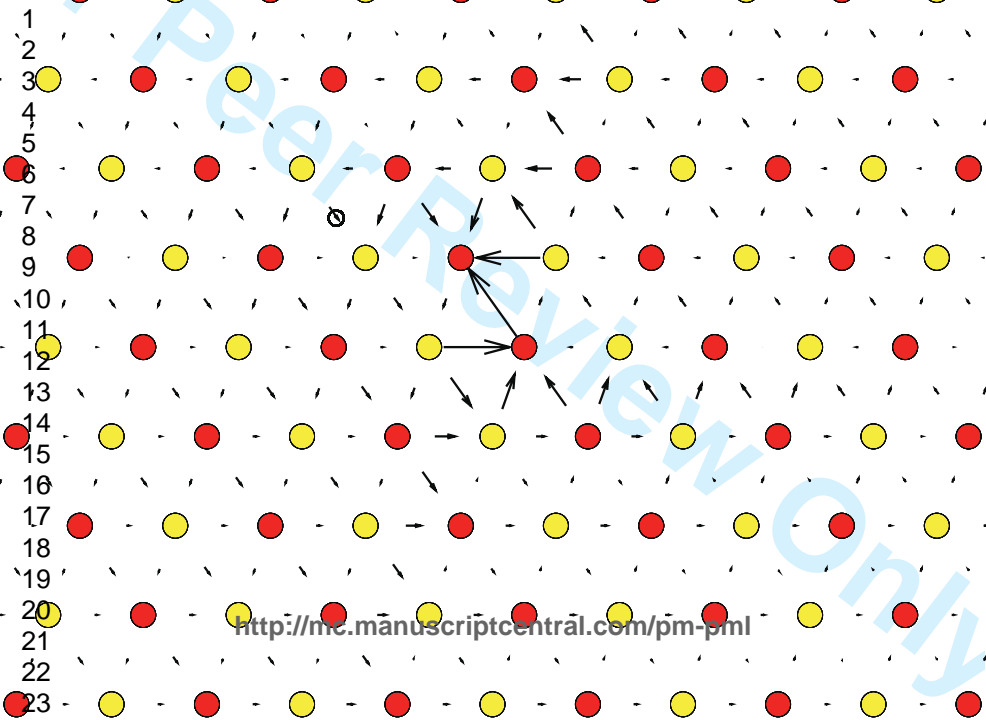
$[\bar{1}\bar{1}2]$

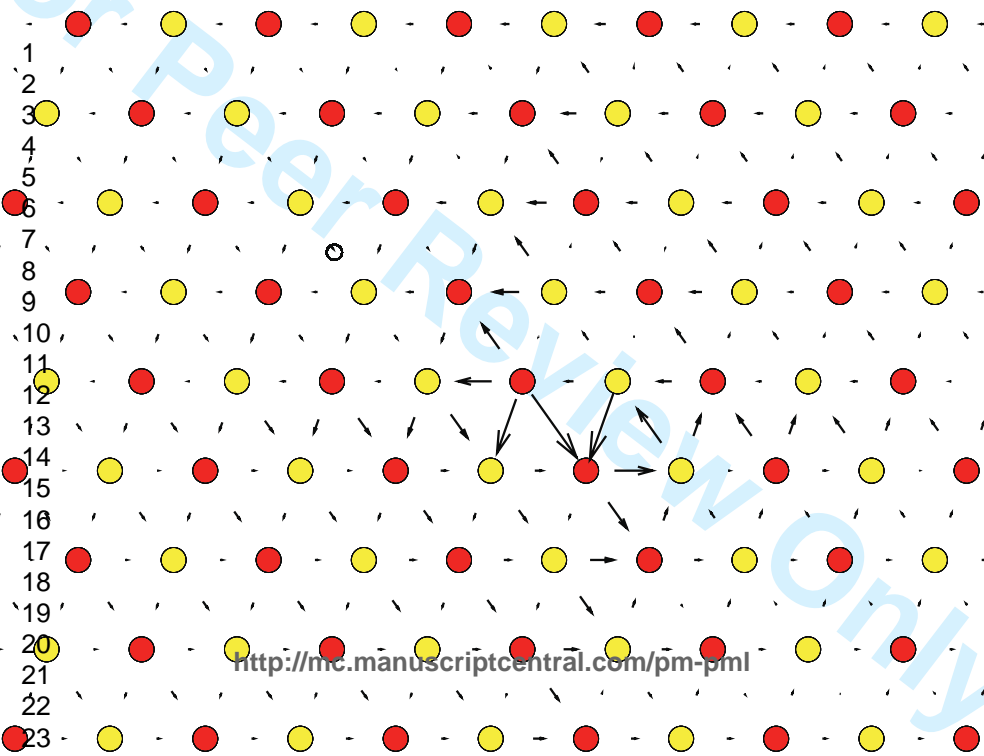
$(11\bar{1})$

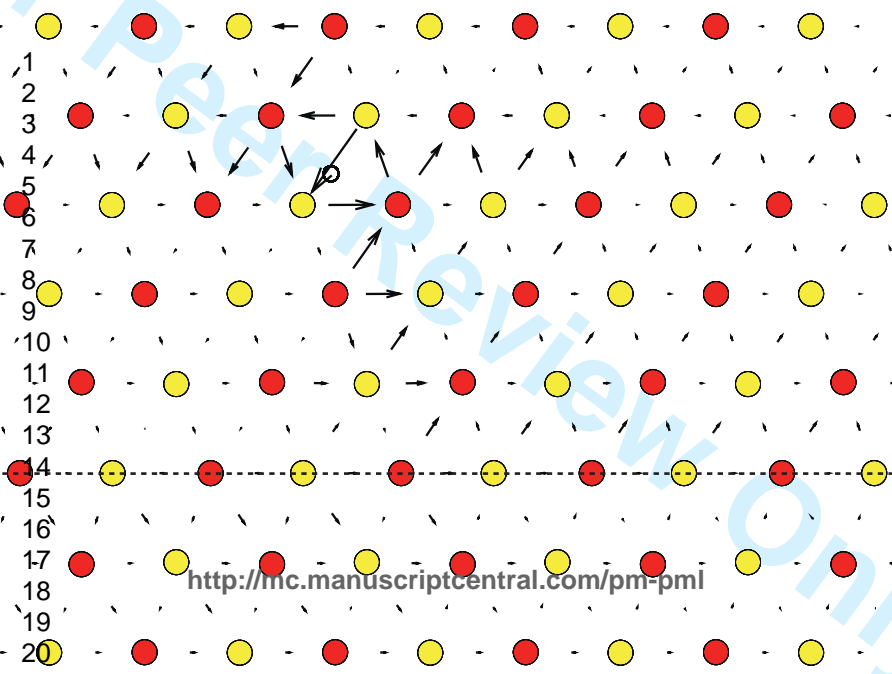
<http://mc.manuscriptcentral.com/pm-pml>

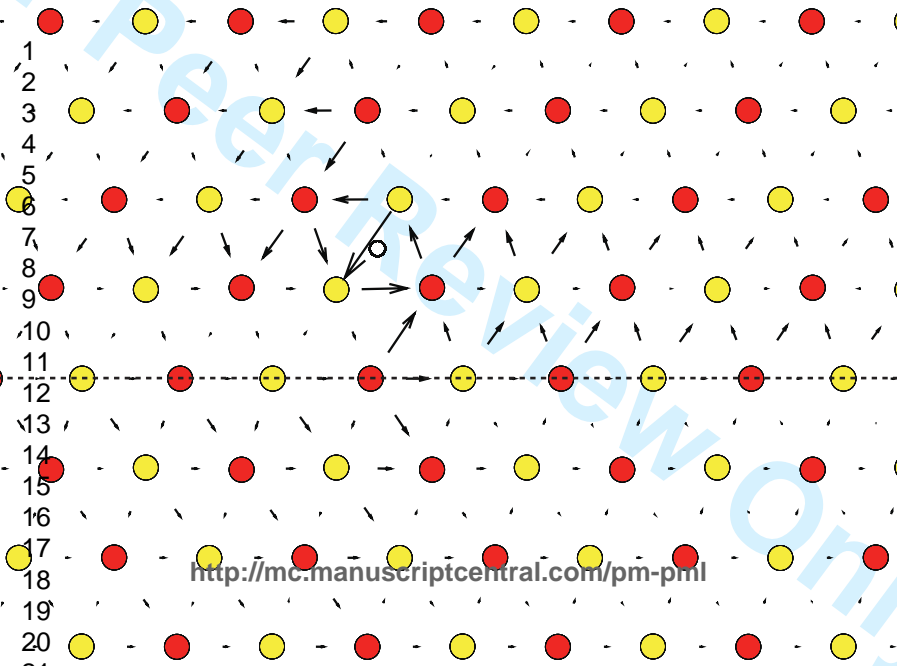


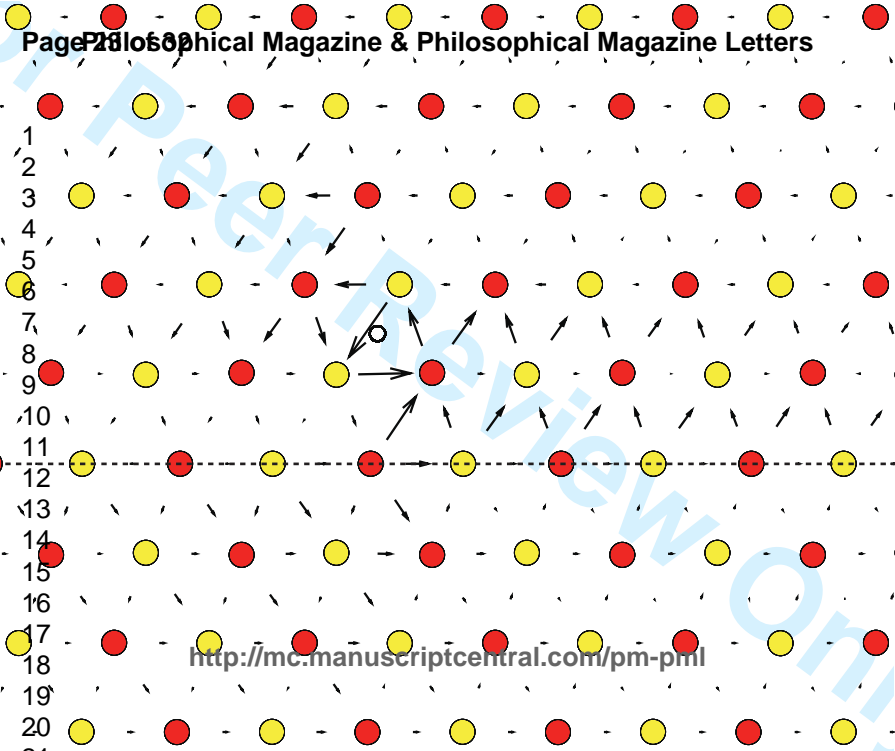


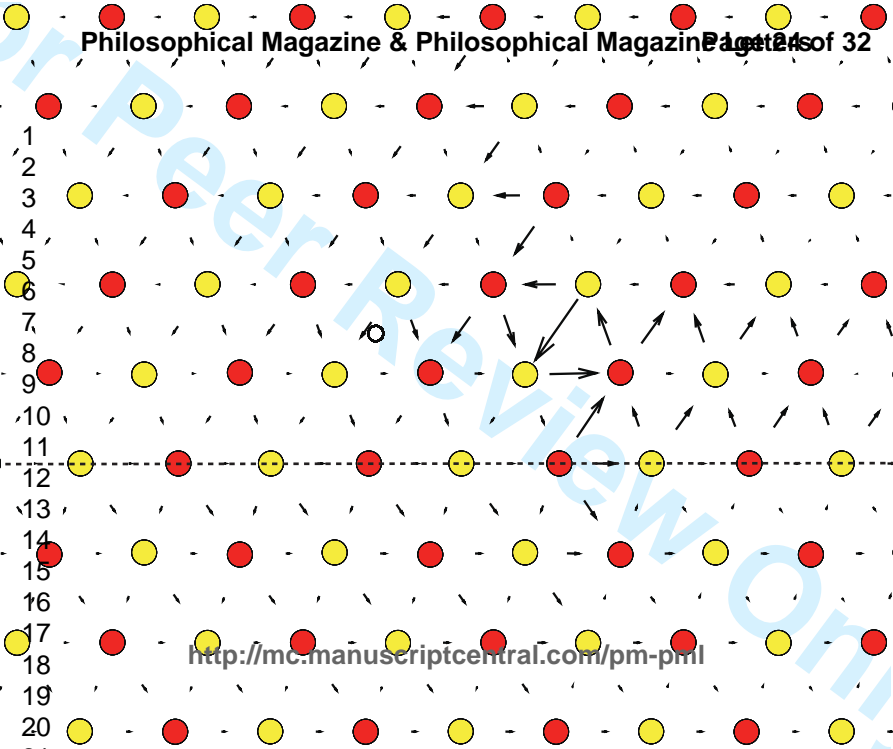


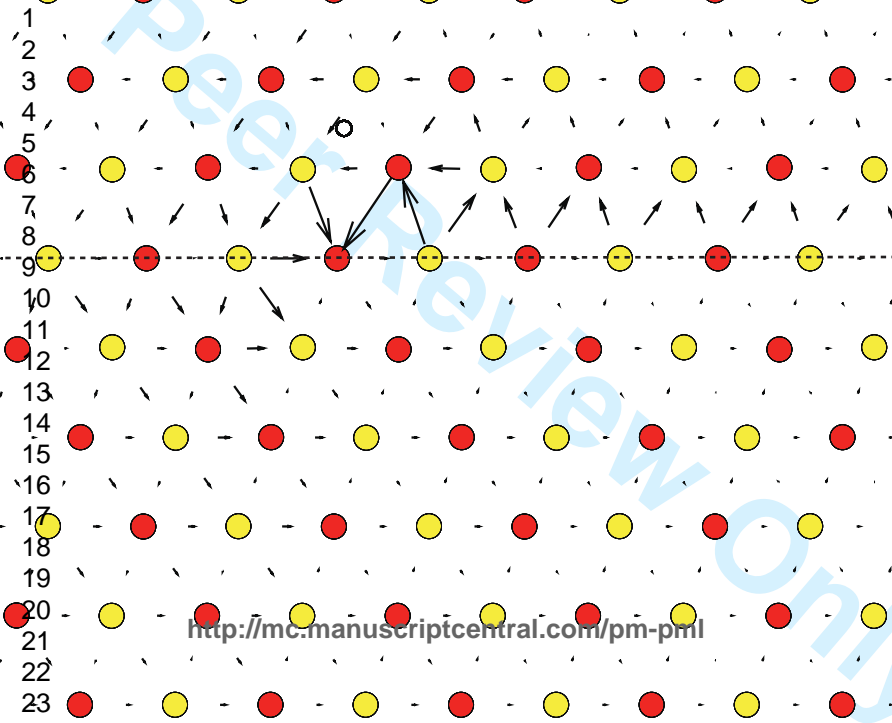


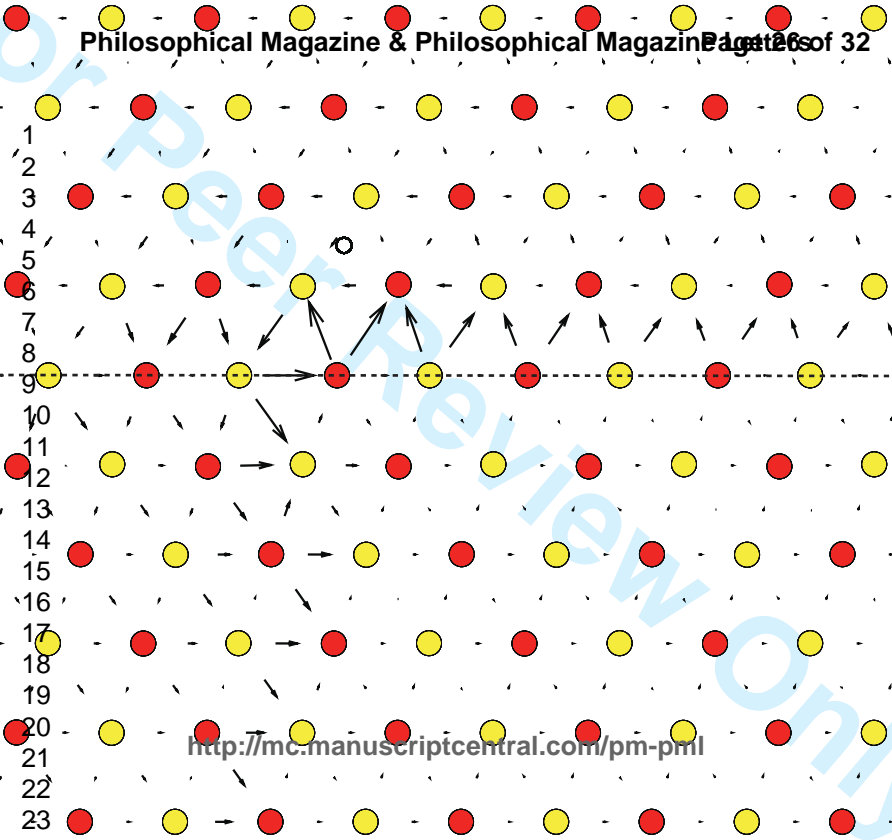




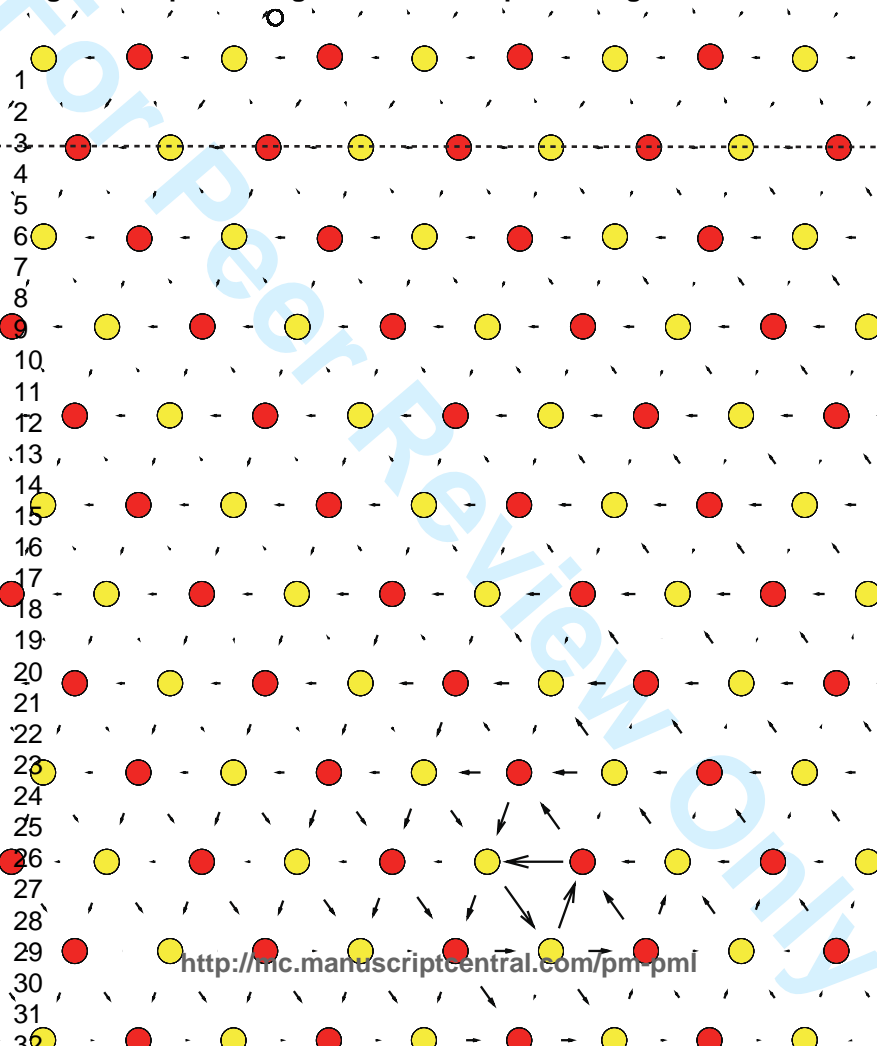


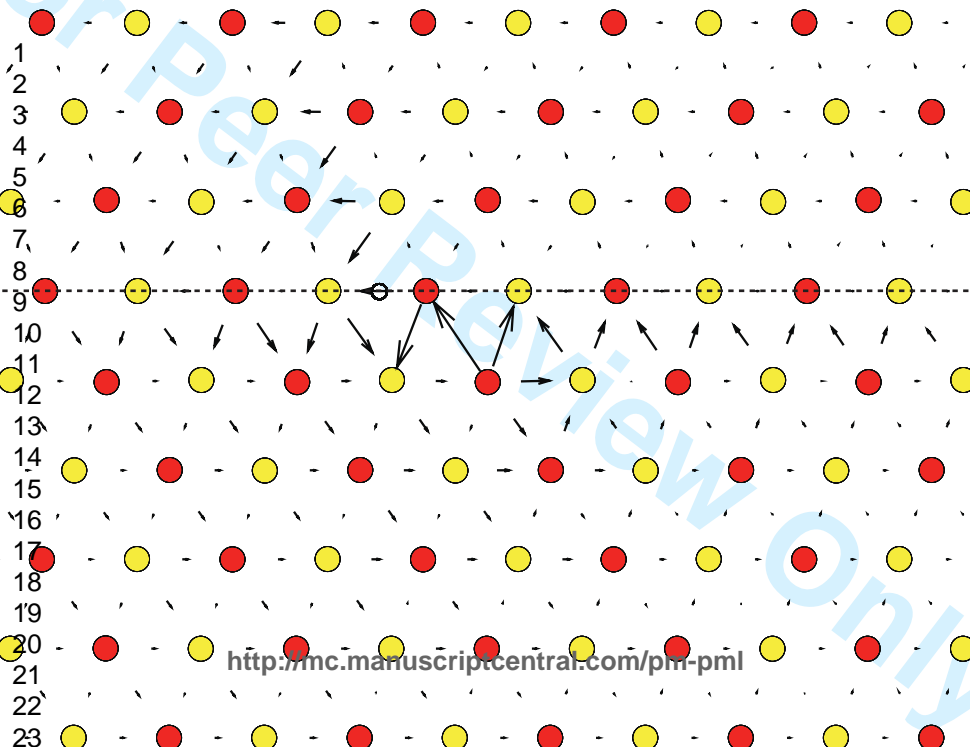






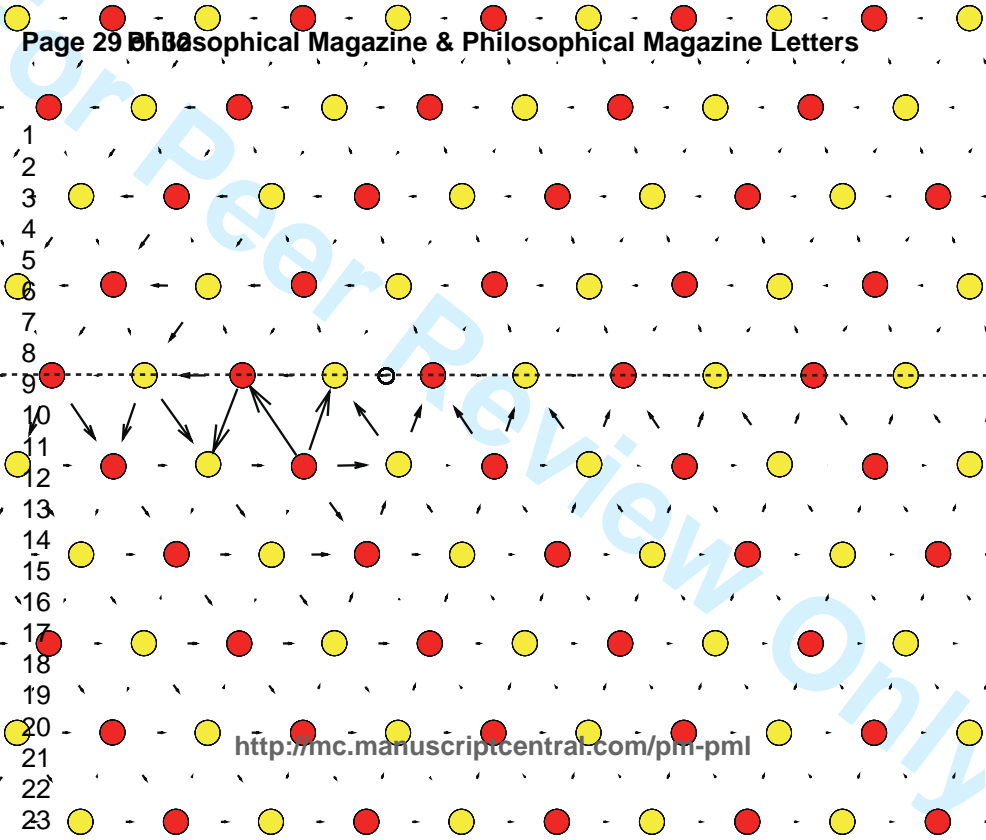
1  
2  
3  
4  
5  
6  
7  
8  
9  
10  
11  
12  
13  
14  
15  
16  
17  
18  
19  
20  
21  
22  
23  
24  
25  
26  
27  
28  
29  
30  
31  
32

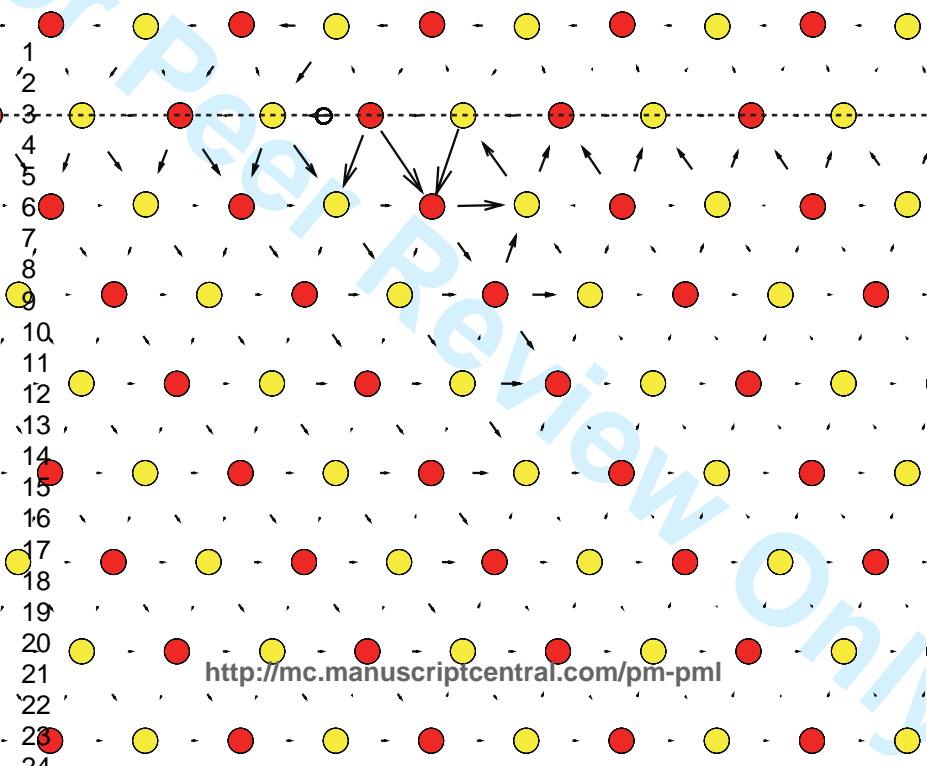




<http://mc.manuscriptcentral.com/pmi-pml>

1  
2  
3  
4  
5  
6  
7  
8  
9  
10  
11  
12  
13  
14  
15  
16  
17  
18  
19  
20  
21  
22  
23





<http://mc.manuscriptcentral.com/pm-pml>

1  
2  
3  
4  
5  
6  
7  
8  
9  
10  
11  
12  
13  
14  
15  
16  
17  
18  
19  
20  
21  
22  
23

